Chinese Journal of Aeronautics, (2023), 36(3): 212–219

Chinese Society of Aeronautics and Astronautics
& Beihang University

Chinese Journal of Aeronautics

cja@buaa.edu.cn
www.sciencedirect.com

Selective thermal emission and infrared camouflage based on layered media

Qingxiang JI [a,b], Xueyan CHEN [a,b], Vincent LAUDE [b], Jun LIANG [c], Guodong FANG [a], Changguo WANG [a,*], Rasoul ALAEE [d,e], Muamer KADIC [b]

[a] National Key Laboratory of Science and Technology on Advanced Composites in Special Environments, Harbin Institute of Technology, Harbin 150001, China
[b] Institute FEMTO-ST, CNRS, University Bourgogne Franche-Comté, Besançon 25000, France
[c] Institute of Advanced Structure Technology, Beijing Institute of Technology, Beijing 100081, China
[d] Department of Physics, University of Ottawa, Ottawa, K1N 6N5, Canada
[e] Institute of Theoretical Solid State Physics, Karlsruhe Institute of Technology, Karlsruhe D-76131, Germany

Received 17 February 2022; revised 10 March 2022; accepted 29 March 2022
Available online 2 September 2022

KEYWORDS

Heat transfer manipulation;
Infrared camouflage;
Multilayer media;
Selective thermal emission;
Thermal illusion;
Transfer matrix method

Abstract Infrared camouflage based on artificial thermal metasurfaces has recently attracted significant attention. By eliminating thermal radiation differences between the object and the background, it is possible to hide a given object from infrared detection. Infrared camouflage is an important element that increases the survivability of aircraft and missiles, by reducing target susceptibility to infrared guided threats. Herein, a simple and practicable design is theoretically presented based on a multilayer film for infrared stealth, with distinctive advantages of scalability, flexible fabrication, and structural simplicity. The multilayer medium consists of silicon substrate, carbon layer and zinc sulfide film, the optical properties of which are determined by transfer matrix method. By locally changing the thickness of the coating film, the spatial tunability and continuity in thermal emission are demonstrated. A continuous change of emissive power is further obtained and consequently implemented to achieve thermal camouflage functionality. In addition, other functionalities, like thermal illusion and thermal coding, are demonstrated by thickness-engineered multilayer films.

1. Introduction

Thermal metamaterials have been designed to realize unusual effective thermal properties in order to create extraordinary devices such as thermal cloaks, concentrators, sensors or illusion devices.[1–21] These devices are based on heat conduction engineering including via the thermal conductivity tensor and the heat capacity. Furthermore, manipulation of out-of-plane

* Corresponding author.
E-mail address: wangcg@hit.edu.cn (C. WANG).
Peer review under responsibility of Editorial Committee of CJA.

Production and hosting by Elsevier

https://doi.org/10.1016/j.cja.2022.08.004
1000-9361 © 2022 Chinese Society of Aeronautics and Astronautics. Production and hosting by Elsevier Ltd.

radiation is more widely studied in radiative cooling and thermal camouflage. Thermal camouflage refers to techniques that make a hot object invisible over the background, which finds potentials in aeronautics, infrared signature suppression and other military applications, i.e., enhances the survivability of aircraft, missiles and even soldiers by evading infrared detection.[22–24]

Thermal camouflage can be realized by matching the detected radiative temperature of an object with its surroundings. By eliminating thermal radiation differences between the object and the background, it is possible to hide or disguise a given object from an infrared camera. According to the Stefan-Boltzmann law, the detected intensity emitted from an object is proportional to the surface emissivity and to the fourth power of the thermodynamic temperature. Therefore, one can achieve thermal camouflage by controlling surface temperatures through transformation thermotics and thermo-regulation systems or by tuning the surface emissivity.[25–32] The latter has the advantage of being passive and that does not require an additional energy source. Currently, infrared stealth has been mainly realized by controlling the surface emissivity using metamaterials or metasurfaces[33–39], phase-changing materials[40–42] and stimuli-responsive structures[43–46,] resulting in adaptive thermal camouflage[47–52] and multispectral camouflage.[53–56]

The thermal metamaterial approach is the main paradigm for infrared camouflage. It requires exploring micro- and nano-structures with well-designed geometries that demonstrate the desired optical properties, which implies complicated fabrication. Besides, this type of surface emissivity control relies on fine tuning the feature size of wavelength-scale structures. It is therefore challenging to obtain a continuously changing surface emissivity. Researchers introduced multilayer medium micro-structures to modulate thermal radiation, which proves easy and flexible for fabrication.[25,35,51,56] However, the reported works have focused on camouflaging a given object with uniform temperature.[33–35,37,39,57] To perfectly camouflage a continuously changing thermal field, which widely exists in practical applications, the required emissivity profile is position-dependent and varies continuously. This problem was tackled by employing a form of discretization, in which a step-wise approximation of ideal emissivity parameters was made at the sacrifice of camouflage performance.[39]

In this work, we propose a simple strategy to realize thermal camouflage based on infrared-transparent thin films thickness engineering. Using this simple approach, we demonstrate spatial tunability and continuity in thermal emission. By locally changing the thickness of the coating film, we obtain a continuous change of emissive power and consequently implement the desired thermal functionalities. This technique of thermal radiation manipulation has the following advantages: (A) In theory, perfect camouflage can be achieved since the required continuously changing thermal radiation can be realized by a calculated thickness distribution that is also continuous, without further discretization and approximation. (B) The same surface emissivity can be obtained with coating films of different thickness, allowing for size flexibility in fabrication. (C) Structural simplicity follows from the fact that only bilayer films are employed.

2. Methods and results

2.1. Working principle of infrared camera

We first recall the working principle of an infrared camera (see Fig. 1). Effective radiation detected by an infrared camera includes three parts, i.e., object radiation $P_{\mathrm{obj}} = \varepsilon_{\mathrm{o}\lambda} P_{\mathrm{b}\lambda}(T_{\mathrm{o}})$, ambient reflection $P_{\mathrm{r}} = R_{\mathrm{o}\lambda} P_{\mathrm{b}\lambda}(T_{\mathrm{a}})$ and air radiation $P_{\mathrm{a}} = \varepsilon_{\mathrm{a}\lambda} P_{\mathrm{b}\lambda}(T_{\mathrm{a}})$, which can be expressed as.

$$P = \tau_{\mathrm{a}\lambda} P_{\mathrm{r}} + P_{\mathrm{a}} + \tau_{\mathrm{a}\lambda} P_{\mathrm{obj}} \tag{1}$$

where $\tau_{\mathrm{a}\lambda}$ and $\varepsilon_{\mathrm{a}\lambda}$ are air transmittance and emissivity respectively, $R_{\mathrm{o}\lambda}$ and $\varepsilon_{\mathrm{o}\lambda}$ are object reflectivity and emissivity respectively, and T_{o} and T_{a} are temperatures of the object and ambient surroundings respectively. $P_{\mathrm{b}\lambda}$ is the black-body radiation received by an infrared camera. The camera transforms the received radiation into signal voltage and further interprets the voltage as scale functions, based on which radiation temperatures are plotted in the camera images. Here we consider "hot objects" where T_{o} and $\varepsilon_{\mathrm{o}\lambda}$ are correspondingly much larger than T_{a} and $R_{\mathrm{o}\lambda}$. Taking a human (skin emissivity 0.97 and body temperature 310 K) in room temperature 293 K as an example, ambient reflection is around only 0.8 % of the object radiation. Besides, air radiation is always small and even negligible. Therefore, in the following work, we modulate thermal emission and realize infrared functionalities mainly by tuning P_{obj}.

2.2. Design scheme

Our design is based on a film-substrate system depicted in Fig. 2(a). Optical properties of the multilayered structure are analytically obtained using the transfer matrix method. The transmission matrix of the j-th layer is expressed as.

$$\boldsymbol{M}_j = \begin{bmatrix} \cos\delta_j & \frac{i}{n_j}\sin\delta_j \\ i n_j \cos\delta_j & \cos\delta_j \end{bmatrix} \tag{2}$$

and the transfer matrix for the whole multilayer film structure, consisting of N layer, reads as.

$$\boldsymbol{M} = \begin{bmatrix} m_{11} & m_{12} \\ m_{21} & m_{22} \end{bmatrix} = \prod_{j=1}^{N} \boldsymbol{M}_j \tag{3}$$

where m_{ij} denote the matrix elements of the transfer matrix for the whole layered media, the refractive index is expressed as $n_j = n_j' + \mathrm{i}n_j''$, and n_j' and n_j'' are the real part and imaginary part, respectively; $\delta_j = 2\pi\lambda^{-1} n_j d_j$ is the effective phase shift thickness of the j-th layer, with d_j being the geometrical thickness and λ the incident wavelength (see details in Appendix A). The reflectivity $R_{\mathrm{o}\lambda}$ and transmissivity $T_{\mathrm{o}\lambda}$ of the multilayer media read as.

$$R_{\mathrm{o}\lambda} = \left|\frac{m_{21}}{m_{11}}\right|^2, T_{\mathrm{o}\lambda} = \left|\frac{m_{22}}{m_{11}}\right|^2 \tag{4}$$

Kirchhoff's law states that the emissivity of an object in thermal equilibrium is equal to its absorptivity $A_{\mathrm{o}\lambda}$, i.e.,

$$\varepsilon_{\mathrm{o}\lambda} = A_{\mathrm{o}\lambda} = 1 - R_{\mathrm{o}\lambda} - T_{\mathrm{o}\lambda} \tag{5}$$

Using Planck's law, the spectral radiance of an object in the atmosphere window is given by.

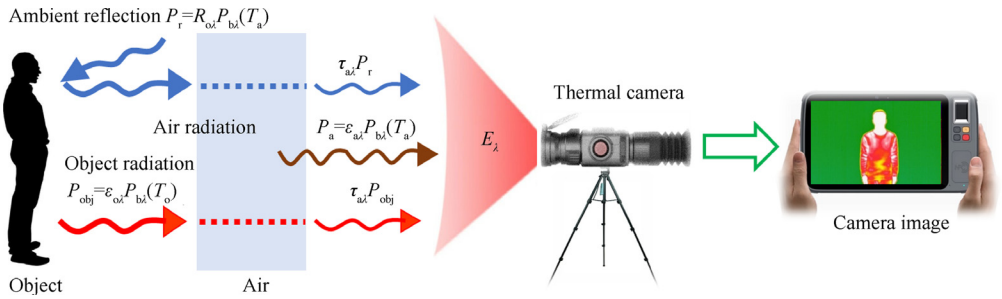

Fig. 1 Working principle of an infrared camera.

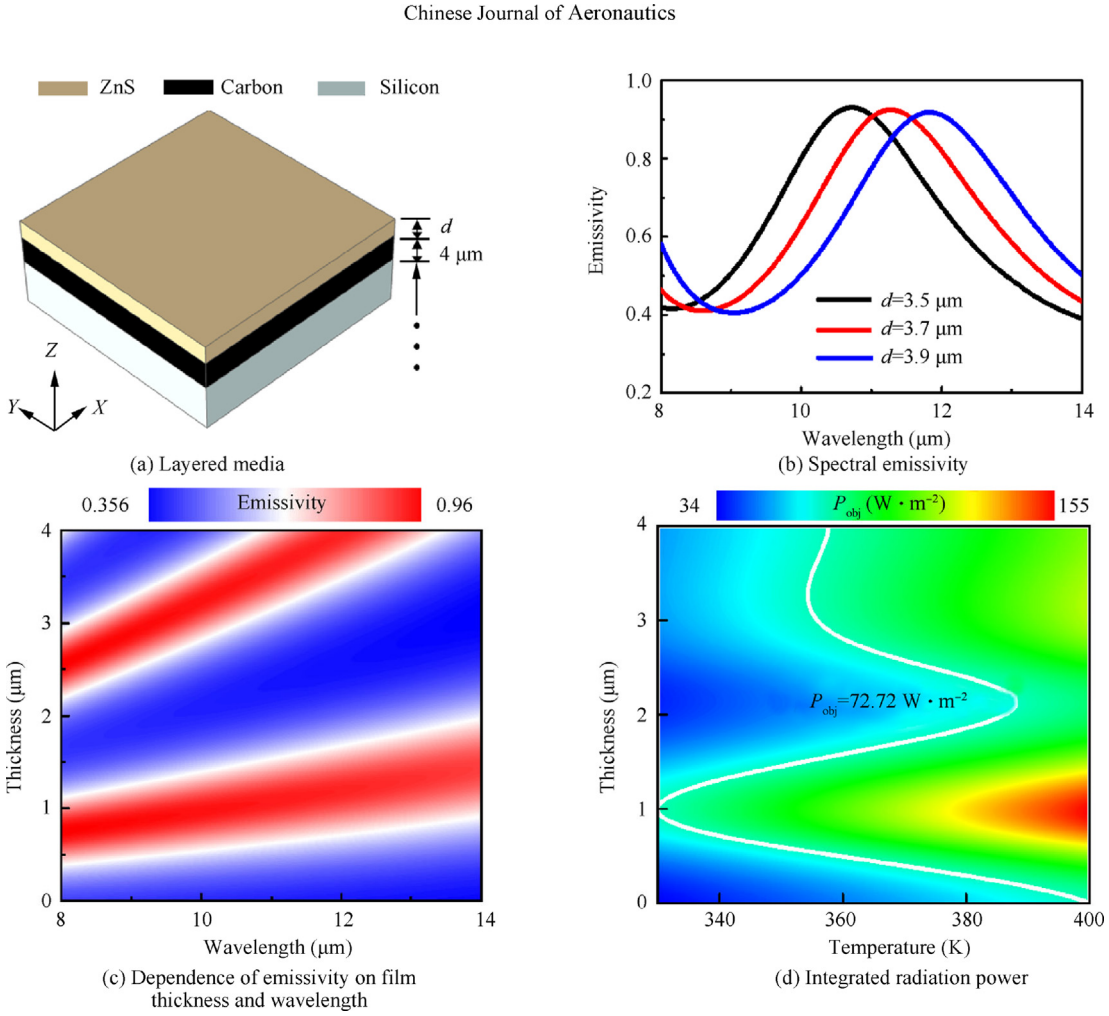

Fig. 2 Optical properties of designed layered media.

$$P_{obj}(T)=\int_{\lambda_1}^{\lambda_2} I_{obj}(\lambda,T)d\lambda=\int_{\lambda_1}^{\lambda_2}\varepsilon_{o\lambda}I_{BB}(\lambda,T)d\lambda \quad (6)$$

where $I_{obj}(\lambda,T)$ is the spectral radiance of the object, $I_{BB}(\lambda,T)=2hc^2\lambda^{-5}(\exp(hc/(\lambda k_B T))-1)^{-1}$ is the spectral radiance of a blackbody at temperature T, h is Planck's constant, k_B is the Boltzmann constant, c is the vacuum speed of light, λ is the wavelength, $\varepsilon_{o\lambda}$ is the spectral emissivity and $[\lambda_1,\lambda_2]$ is the spectral range of the infrared camera. Note that the operating wavelength range for an infrared thermal camera is often 3–5 μm or 8–14 μm. Outside those two windows, infrared radiation is mostly attenuated by the surrounding air.

Eq. (6) demonstrates that the perceived radiation by an infrared camera can be effectively tuned by engineering the emissivity of the metasurface. A thermal infrared camera integrates the received energy over its operational wavelength and transfers the integration values to the recorded temperatures in thermal images, which can be expressed by.

$$T_r = \phi_\lambda P_{obj}(T) = \phi_\lambda \int_{\lambda_1}^{\lambda_2} \varepsilon_{o\lambda} I_{BB}(\lambda, T) d\lambda \quad (7)$$

where ϕ_λ is a parameter related to the lens area and spectral responsivity of an infrared camera. ϕ_λ is invariant for a given infrared camera.[41] The detected temperature T_r of an object recorded in infrared images is equal to the real temperature T if and only if the object is a black-body and the air transmittance $\tau_{a\lambda} = 1$. T_r is directly related to $P_{obj}(T)$ which is dependent on both the emissivity ε_{obj} (tuned by the film thickness d in this work) and the real temperature T. To achieve perfect thermal camouflage, the recorded temperature T_r (or $P_{obj}(T)$) should be spatially constant. Considering that each surface unit has a different temperature, we tune the spectral emissivity of each unit to make T_r (or $P_{obj}(T)$) the same over the whole sample by depositing over each unit a thin film of the corresponding thickness. We emphasize that the proposed strategy is also applicable to thermal radiation illusion or coding.

2.3. Design method

We now realize thermal radiation modulation by engineering optical properties of the surface. For clarity, the design process for the general case is outlined through a specific example. Let us focus on the integrated radiation power $P_{obj}(T)$ in the operating wavelength range 8–14 μm that is directly related to the observed temperatures in the infrared images of the infrared camera. We choose carbon as the ground layer with a thickness of 4 μm, leading to zero transmission $T_{o\lambda} = 0$. Silicon is chosen as a substrate. Then, we use a dielectric layer made of zinc sulfide (ZnS) as a transparent material within the range of wavelengths 8–14 μm (see Fig. 2(a)), and the optical properties are from Refs. 37,58 On the basis of energy balance, we calculate the emissivity from Eq. (5). Spectral emissivity for various film thicknesses is shown in Fig. 2(b) and (c). With an increment of film thickness from 3.5 μm to 3.9 μm, the emissivity peak shifts from 0.93 at wavelength 10.7 μm to 0.92 at wavelength 11.8 μm. The emissivity as a function of thickness of ZnS and wavelength is depicted in Fig. 2(c). It can be seen that one can control the emissivity by engineering the thickness of ZnS. Within the wavelength range 8–14 μm, the emissivity varies from 0.356 to 0.96. It is noted that other materials may also be considered to design the multilayer medium structure shown in Fig. 2(a). For instance, if we replace ZnS with germanium, the emissivity varies from 0.351 to 0.941, which is almost the same as for ZnS. The selection of film materials should be made so that the tailorable emissivity range is as large as possible. Optical properties of the selected materials are shown in the supporting information. We conduct finite element analysis to verify the calculated spectral emissivity for the designed multilayer media, as shown in Fig. 2(b). The Finite Element Analysis (FEA) results perfectly agree with the results predicted by Eq. (5). The simulation is conducted by the commercial software COMSOL Multiphysics with the optics module. The unit cell in Fig. 2(a) is modeled except for the silicon substrate, because the carbon layer here ensures zero transmittance. For the simulation of the EM behavior, the excitation Electromagnetics (EM) wave propagates along the z-axis as a plane wave. From the simulation results, we obtain the S-parameters and further obtain the reflectivity and transmittivity. Absorptivity/emissivity is finally got on the basis of energy balance and Kirchhoff's law.

Using Eq. (6), the radiated power is calculated as a function of ZnS thickness and temperature (see Fig. 2(d)). For example, the integrated power $P_{obj}(T) = 72.72\ W \cdot m^{-2}$ is shown by a white iso-contour line in Fig. 2(d). Objects having temperatures spanning the range 330–400 K would be effectively detected to have the same emissive power if their surfaces were deposited with a dielectric layer whose thickness is determined by the corresponding white iso-contour line.

In the following, we outline the process to achieve camouflage functionality based on the multilayer medium approach. Fig. 3(a) shows a continuous temperature distribution generated by imposing temperature difference $\Delta T = 40$ K at the two ends of the silicon substrate (thermal conductivity $k_s = 1.3\ W \cdot m^{-1} \cdot K^{-1}$). The side length of the simulated plate is 100 mm. The surface is in contact with air with natural convection coefficient $2\ W \cdot m^{-2} \cdot K^{-1}$ at temperature 340 K. We plot the temperature at different × positions in Fig. 3(b). Note that the temperature is uniform along the y direction. Fig. 3(c) shows the integrated radiation power at three typical positions along the observed line (namely A, B and C), where it is observed that higher temperatures result in larger radiation powers, in general. The first step is to select a desired radiation power P_{obj} that all points can achieve with a selected film thickness. The possible range of the integrated radiation power is outlined in grey area. The camouflaged temperatures range from 340 K to 380 K (see Fig. 3(b)). We select the thickness profile shown in Fig. 3(d) for $P_{obj}(T) = 72.72\ W \cdot m^{-2}$. The observed uniform camera temperature is shown in Fig. 3(a) with black line for the designed film with inhomogeneous thickness. The camera temperature field is obtained using Eq. (7), where ϕ_λ is obtained using blackbody radiation. Therefore, the heat spot located at the center is hidden for an infrared camera. This illustrating case demonstrates the thermal camouflage functionality by selective emission and thickness engineering. Note that other integrated radiation powers are also applicable if and only if they fall into the grey area. The difference is that we will obtain different thickness distributions with those in Fig. 3(d) and further observe different detected camera temperatures with those in Fig. 3(b), as may be predicted by Eq. (7). For a selected integrated radiation power, there exist not only one set of potential thickness distribution that can realize thermal camouflage effects. We marked, in Fig. 3(c), two groups of available film thickness that can achieve the same integrated radiation power and hence the same emission modulation performance. This size flexibility will add much convenience to practical applications.

3. Results and discussion

Based on the approach above, we can engineer the whole surface emissivity (thickness) to realize thermal functionalities such as camouflage, illusion, and coding (see Fig. 4). In Fig. 4(a)–(c), thermal camouflage functionality is demonstrated. We aim to thermally hide a heat source of radius 2 mm located at the center of the silicon substrate. The required layer thickness is the smallest at the central position and increases from the center outward, as shown in Fig. 4 (b). The camera temperature field is uniform ($T_r = 319.8$ K)

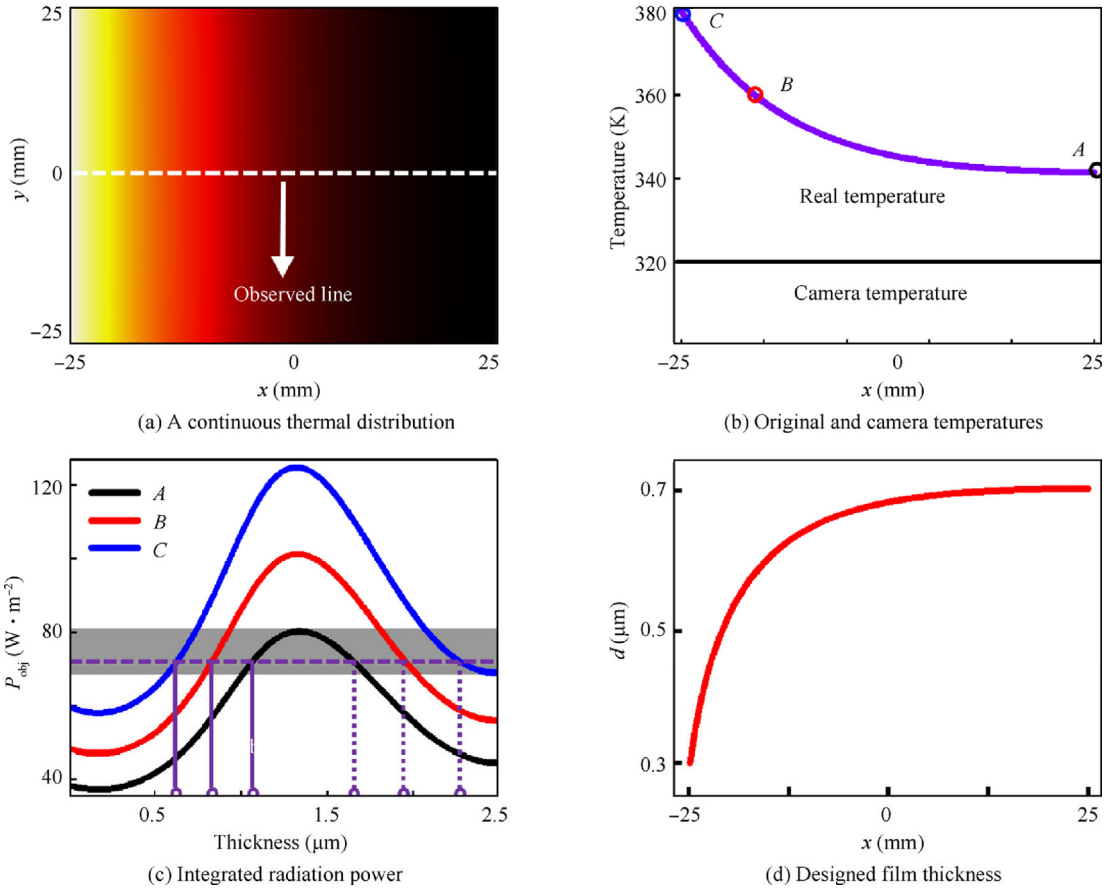

Fig. 3 Outline of the process to realize thermal camouflage.

after film deposition, and thus the heat spot in the background plate is invisible to the detector, demonstrating perfect camouflage functionality, as shown in Fig. 4(c).

By tailoring the distribution of the thickness of the coating film, we further obtain the thermal coding functionality in Fig. 4(d)–(f). In a uniform thermal field with $T = 360$ K (see Fig. 4(d)), we leave out a sub-area "HI" and deposit a coating layer of thickness 0.5 μm everywhere else (see Fig. 4(e)). As a result, the heat signature "HI" (camera temperature 360 K) emerges from the background thermal field (camera temperature 319.8 K depicted in Fig. 4(f)). We determine coating layer thicknesses using the radiation power of $P_{obj}(T) = 72.72\ \mathrm{W \cdot m^{-2}}$.

We then demonstrate the thermal illusion functionality in Fig. 4(g)–(i), where the heat signature "NO" is observed instead of the original message "YES" to confuse observers. This illusion functionality is also realized by properly engineering the film thickness. The surface is divided into three sub-regions: "YES", "NO", and background (see Fig. 4(h)). We deposit the sub-regions "YES" and background with film thicknesses 0.3 μm and 0.5 μm, respectively, whereas sub-region "NO" remains uncoated. After deposition, the sign "NO" will be observed in the camera image instead of the original sign "YES" (see Fig. 4(i)). We emphasize that more functionalities can be obtained through the proposed flexible film thickness engineering strategy.

In our design, a very important aspect is the huge scale difference between variations of physical quantities (such as the temperature) inside the layer thickness and in the lateral directions. However, the layer thickness is of the order of a few microns, and the thermal gradient and thus the thermal distribution only change significantly over very large lateral distances. Considering a meter-size object and a temperature difference between the two sides of $\Delta T = 100$ K, then at the scale of a typical infrared wavelength of 10 μm, the temperature change is only about 10^{-3} K. At that scale, the temperature variation can be considered continuous and the local change in thickness will not lead to any significant lateral scattering. Based on this reasoning, in the coding and illusion devices depicted in Fig. 4(d)–(f) and Fig. 4(g)–(i), the apparent discontinuities in the thickness and temperature can be made continuous to avoid scattering from the edges. Here we have ignored this aspect in the plots as the discontinuities can be smoothed out easily. In addition, thermal conduction in the slab when varying the local thickness is also neglected. Consider the camouflage case in Fig. 4(a)–(c) where the silicon plate is built with thermal conductivity $k_s = 1.3\ \mathrm{W \cdot m^{-1} \cdot K^{-1}}$ and thickness 2 mm. The surface is coated with a ZnS layer with thermal conductivity $25\ \mathrm{W \cdot m^{-1} \cdot K^{-1}}$ and a typical thickness 0.7 μm. Assume that the temperature range is 1 K in the thickness direction, and then the temperature over the ZnS layer thickness direction

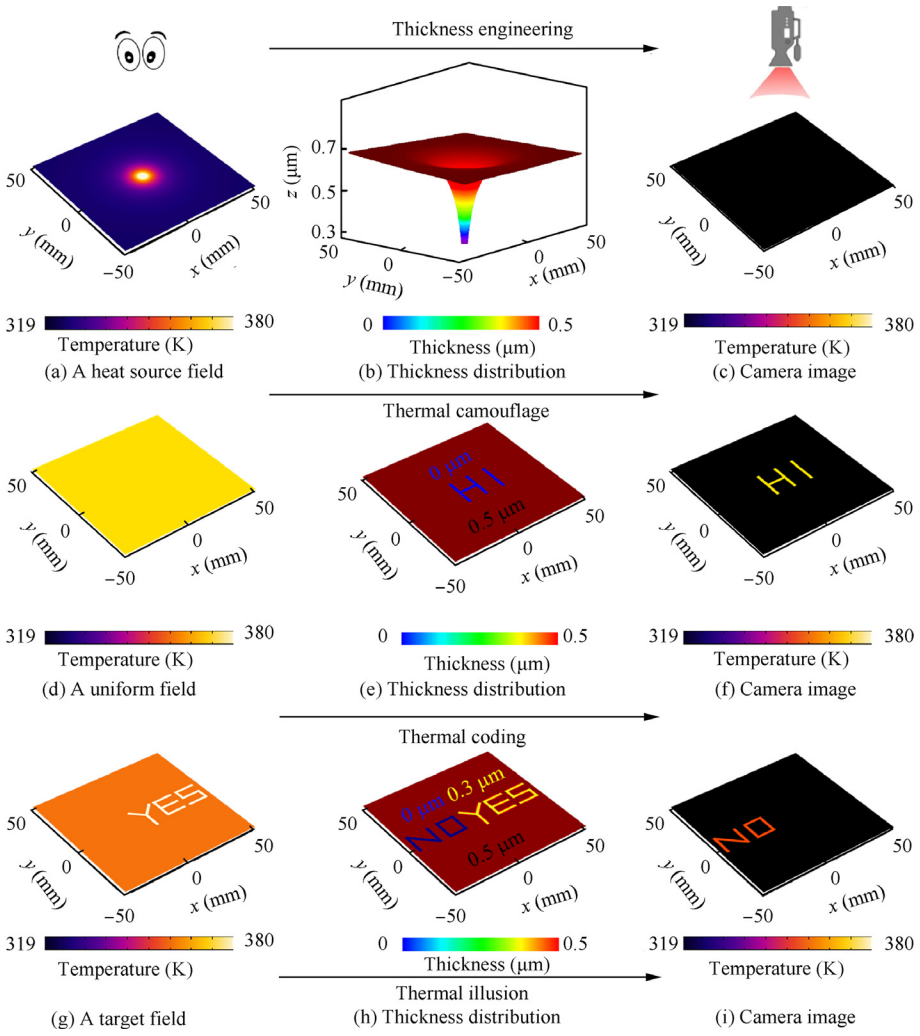

Fig. 4 Demonstration of different thermal functionalities.

only changes by 2.6×10^{-5} K which is negligible and makes few influences on the radiation power. Therefore, surface temperature difference due to conduction is safely ignored.

In this work, we achieve selective emission based on thin film thickness engineering with predefined materials, yet practical implementation may demand diversity in design parameters due to the possible unavailability of material properties and manufacture deviations. Therefore, in the next step we will consider to obtain selective emission based on machine learning, which will intelligently establish the relation between deign parameters (film properties, thickness, etc.) and emissivity spectrum.[16,59–62] Such a data driven approach will demonstrate flexibility and accuracy in realizing functionalities like thermal camouflage, illusion and so on.

4. Conclusions

A multilayer film based selective emission strategy was proposed and investigated for applications in infrared camouflage, thermal coding and thermal illusion. Through thickness engineering, the emissivity can be tuned continuously over a large range. The technique features advantages of a simple structure, easy fabrication and size flexibility. Our work provides an alternative solution to infrared stealth and other thermal radiation management technology based on selective emission. From the current study, the following conclusions are drawn.

1. For the established multilayer medium, the surface emissivity can be tuned from 0.356 to 0.96 within the wavelength range 8–14 μm, by changing the film thickness. Using this multilayer media approach, spatial tunability and continuity in thermal emission are demonstrated.
2. Perfect camouflage can be achieved since the required continuously changing thermal radiation is realized by a calculated thickness distribution that is also continuous, without further discretization and approximation. For a given heat source, different solutions of film thickness are applicable, allowing for size flexibility in practical implementation.
3. Other thermal functionalities, i.e., thermal coding and thermal illusion, are also realized by simple film thickness engineering, following structural simplicity.

Declaration of Competing Interest

The authors declare that they have no known competing financial interests or personal relationships that could have appeared to influence the work reported in this paper.

Acknowledgements

This work was supported by the EIPHI Graduate School (No. ANR-17-EURE-0002), the French Investissements d'Avenir program, project ISITEBFC (No. ANR-15-IDEX-03), and the National Natural Science Foundation of China (Nos. 12172102, 11872160 and 11732002). Rasoul ALAEE acknowledges the support of the Alexander von Humboldt Foundation through the Feodor Lynen Fellowship.

Appendix A. Supplementary material

Supplementary data to this article can be found online at https://doi.org/10.1016/j.cja.2022.08.004.

References

1. Fan CZ, Gao Y, Huang JP. Shaped graded materials with an apparent negative thermal conductivity. *Appl Phys Lett* 2008;**92**(25):251907.
2. Guenneau S, Amra C, Veynante D. Transformation thermodynamics: cloaking and concentrating heat flux. *Opt Express* 2012;**20**(7):8207–18.
3. Guenneau S, Amra C. Anisotropic conductivity rotates heat fluxes in transient regimes. *Opt Express* 2013;**21**(5):6578–83.
4. Kadic M, Bückmann T, Schittny R, et al. Metamaterials beyond electromagnetism. *Rep Prog Phys Phys Soc G B* 2013;**76**(12):126501.
5. Schittny R, Kadic M, Guenneau S, et al. Experiments on transformation thermodynamics: molding the flow of heat. *Phys Rev Lett* 2013;**110**(19):195901.
6. Shen XY, Huang JP. Thermally hiding an object inside a cloak with feeling. *Int J Heat Mass Transf* 2014;**78**:1–6.
7. Han TC, Bai X, Thong JTL, et al. Full control and manipulation of heat signatures: cloaking, camouflage and thermal metamaterials. *Adv Mater* 2014;**26**(11):1731–4.
8. Fleury R, Monticone F, Alù A. Invisibility and cloaking: origins, present, and future perspectives. *Phys Rev Appl* 2015;**4**(3):037001.
9. Fleury R, Sounas D, Alù A. An invisible acoustic sensor based on parity-time symmetry. *Nat Commun* 2015;**6**:5905.
10. Yang TZ, Bai X, Gao DL, et al. Invisible sensors: simultaneous sensing and camouflaging in multiphysical fields. *Adv Mater* 2015;**27**(47):7752–8.
11. Zhou SL, Hu R, Luo XB. Thermal illusion with twinborn-like heat signatures. *Int J Heat Mass Transf* 2018;**127**:607–13.
12. Han TC, Yang P, Li Y, et al. Full-parameter omnidirectional thermal metadevices of anisotropic geometry. *Adv Mater* 2018;**30**(49):1804019.
13. Hu R, Zhou SL, Li Y, et al. Illusion thermotics. *Adv Mater* 2018;**30**(22):1707237.
14. Hu R, Huang SY, Wang M, et al. Binary thermal encoding by energy shielding and harvesting units. *Phys Rev Appl* 2018;**10**(5):054032.
15. Hu R, Huang SY, Wang M, et al. Encrypted thermal printing with regionalization transformation. *Adv Mater* 2019;**31**(25):1807849.
16. Hu R, Song JL, Liu YD, et al. Machine learning-optimized Tamm emitter for high-performance thermophotovoltaic system with detailed balance analysis. *Nano Energy* 2020;**72**:104687.
17. Ji QX, Chen XY, Liang J, et al. Designing thermal energy harvesting devices with natural materials through optimized microstructures. *Int J Heat Mass Transf* 2021;**169**:120948.
18. Sha W, Xiao M, Zhang JH, et al. Robustly printable freeform thermal metamaterials. *Nat Commun* 2021;**12**:7228.
19. Zhu Z, Ren XC, Sha W, et al. Inverse design of rotating metadevice for adaptive thermal cloaking. *Int J Heat Mass Transf* 2021;**176**:121417.
20. Hu R, Zhou SL, Shu WC, et al. Directional heat transport through thermal reflection meta-device. *AIP Adv* 2016;**6**(12):125111.
21. Zhao WX, Zhu Z, Fan YW, et al. Temporally-adjustable radiative thermal diode based on metal-insulator phase change. *Int J Heat Mass Transf* 2022;**185**:122443.
22. Pan CX, Zhang JZ, Shan Y. Modeling and analysis of helicopter thermal and infrared radiation. *Chin J Aeronaut* 2011;**24**(5):558–67.
23. Yang ZY, Zhang JZ, Shan Y. Effects of forward-flight speed on plume flow and infrared radiation of IRS-integrating helicopter. *Chin J Aeronaut* 2022;**35**(3):155–68.
24. Zhou Y, Wang Q, Li T. A new model to simulate infrared radiation from an aircraft exhaust system. *Chin J Aeronaut* 2017;**30**(2):651–62.
25. Xiao L, Ma H, Liu JK, et al. Fast adaptive thermal camouflage based on flexible VO_2/graphene/CNT thin films. *Nano Lett* 2015;**15**(12):8365–70.
26. Li Y, Bai X, Yang TZ, et al. Structured thermal surface for radiative camouflage. *Nat Commun* 2018;**9**:273.
27. Hong S, Shin S, Chen RK. An adaptive and wearable thermal camouflage device. *Adv Funct Mater* 2020;**30**(11):1909788.
28. Peng YG, Li Y, Cao PC, et al. 3D printed meta-helmet for wide-angle thermal camouflages. *Adv Funct Mater* 2020;**30**(28):2002061.
29. Liu Y, Song J, Zhao W, et al. Dynamic thermal camouflage via a liquid-crystal-based radiative metasurface. *Nanophotonics* 2020;**9**(4):855–63.
30. Hu R, Xi W, Liu YD, et al. Thermal camouflaging metamaterials. *Mater Today* 2021;**45**:120–41.
31. Zhang JW, Huang SY, Hu R. Adaptive radiative thermal camouflage via synchronous heat conduction. *Chin Phys Lett* 2021;**38**(1):010502.
32. Liu YD, Zuo HY, Xi W, et al. Flexible Janus functional film for adaptive thermal camouflage. *Adv Mater Technol* 2022;**7**(3):2100821.
33. Ueba Y, Takahara J. Spectral control of thermal radiation by metasurface with split-ring resonator. *Appl Phys Express* 2012;**5**(12):122001.
34. Moghimi MJ, Lin GY, Jiang HR. Broadband and ultrathin infrared stealth sheets. *Adv Eng Mater* 2018;**20**(11):1800038.
35. Peng L, Liu DQ, Cheng HF, et al. A multilayer film based selective thermal emitter for infrared stealth technology. *Adv Opt Mater* 2018;**6**(23):1801006.
36. Xie X, Li X, Pu MB, et al. Plasmonic metasurfaces for simultaneous thermal infrared invisibility and holographic illusion. *Adv Funct Mater* 2018;**28**(14):1706673.
37. Lee N, Kim T, Lim JS, et al. Metamaterial-selective emitter for maximizing infrared camouflage performance with energy dissipation. *ACS Appl Mater Interfaces* 2019;**11**(23):21250–7.
38. Wang D, Zhu YQ, Fang C, et al. Example of metal-multi-dielectric-metal cooling metamaterial use in engineering thermal radiation. *Appl Opt* 2019;**58**(26):7035–41.
39. Song JL, Huang SY, Ma YP, et al. Radiative metasurface for thermal camouflage, illusion and messaging. *Opt Express* 2020;**28**(2):875–85.

40. Salihoglu O, Uzlu HB, Yakar O, et al. Graphene-based adaptive thermal camouflage. *Nano Lett* 2018;**18**(7):4541–8.
41. Qu YR, Li Q, Cai L, et al. Thermal camouflage based on the phase-changing material GST. *Light Sci Appl* 2018;**7**:26.
42. Lyu J, Liu ZW, Wu XH, et al. Nanofibrous kevlar aerogel films and their phase-change composites for highly efficient infrared stealth. *ACS Nano* 2019;**13**(2):2236–45.
43. Vassant S, Moldovan Doyen I, Marquier F, et al. Electrical modulation of emissivity. *Appl Phys Lett* 2013;**102**(8):081125.
44. Liu XY, Padilla WJ. Thermochromic infrared metamaterials. *Adv Mater* 2016;**28**(5):871–5.
45. Krishna A, Kim JM, Leem J, et al. Ultraviolet to mid-infrared emissivity control by mechanically reconfigurable graphene. *Nano Lett* 2019;**19**(8):5086–92.
46. Zhang XA, Yu SJ, Xu BB, et al. Dynamic gating of infrared radiation in a textile. *Science* 2019;**363**(6427):619–23.
47. Inoue T, de Zoysa M, Asano T, et al. Realization of dynamic thermal emission control. *Nat Mater* 2014;**13**(10):928–31.
48. Brar VW, Sherrott MC, Jang MS, et al. Electronic modulation of infrared radiation in graphene plasmonic resonators. *Nat Commun* 2015;**6**:7032.
49. Cui Y, Gong HX, Wang YJ, et al. A thermally insulating textile inspired by polar bear hair. *Adv Mater* 2018;**30**(14):1706807.
50. Xu CY, Stiubianu GT, Gorodetsky AA. Adaptive infrared-reflecting systems inspired by cephalopods. *Science* 2018;**359**(6383):1495–500.
51. Tang KC, Wang X, Dong KC, et al. A thermal radiation modulation platform by emissivity engineering with graded metal-insulator transition. *Adv Mater* 2020;**32**(36):1907071.
52. Li MY, Liu DQ, Cheng HF, et al. Manipulating metals for adaptive thermal camouflage. *Sci Adv* 2020;**6**(22):eaba3494.
53. Chandra S, Franklin D, Cozart J, et al. Adaptive multispectral infrared camouflage. *ACS Photon* 2018;**5**(11):4513–9.
54. Kim T, Bae JY, Lee N, et al. Hierarchical metamaterials for multispectral camouflage of infrared and microwaves. *Adv Funct Mater* 2019;**29**(10):1807319.
55. Pan MY, Huang Y, Li Q, et al. Multi-band middle-infrared-compatible camouflage with thermal management via simple photonic structures. *Nano Energy* 2020;**69**:104449.
56. Zhu HZ, Li Q, Tao CN, et al. Multispectral camouflage for infrared, visible, lasers and microwave with radiative cooling. *Nat Commun* 2021;**12**:1805.
57. Liu N, Mesch M, Weiss T, et al. Infrared perfect absorber and its application as plasmonic sensor. *Nano Lett* 2010;**10**(7):2342–8.
58. Debenham M. Refractive indices of zinc sulfide in the 0.405-13-mgrm wavelength range. *Appl Opt* 1984;**23**(14):2238.
59. Hu R, Iwamoto S, Feng L, et al. Machine-learning-optimized aperiodic superlattice minimizes coherent phonon heat conduction. *Phys Rev X* 2020;**10**(2):021050.
60. Xi W, Liu YD, Zhao WX, et al. Colored radiative cooling: how to balance color display and radiative cooling performance. *Int J Therm Sci* 2021;**170**:107172.
61. Xi W, Liu YD, Song JL, et al. High-throughput screening of a high-Q mid-infrared Tamm emitter by material informatics. *Opt Lett* 2021;**46**(4):888–91.
62. Ji QX, Qi YC, Liu CW, et al. Design of thermal cloaks with isotropic materials based on machine learning. *Int J Heat Mass Transf* 2022;**189**:122716.